Chemical Engineering Journal 322 (2017) 454–462

Contents lists available at ScienceDirect

Chemical Engineering Journal

journal homepage: www.elsevier.com/locate/cej

Caterpillar-like graphene confining sulfur by restacking effect for high performance lithium sulfur batteries

Guiyin Xu [a,b,1], Jiaren Yuan [b,1], Xiumei Geng [a], Hui Dou [b,*], Liao Chen [a], Xiaohong Yan [c], Hongli Zhu [a,*]

[a] Department of Mechanical and Industrial Engineering, Northeastern University, Boston, MA 02115, USA
[b] Jiangsu Key Laboratory of Material and Technology for Energy Conversion, College of Material Science and Engineering, Nanjing University of Aeronautics and Astronautics, Nanjing 210016, China
[c] College of Electronic Science and Engineering, Nanjing University of Posts and Telecommunications, Nanjing 210046, China

HIGHLIGHTS

- Hierarchical and porous graphene as sulfur host was obtained from graphite.
- The graphene could effectively trap sulfur by the Van der waals restacking effect.
- The graphene/sulfur cathode exhibited high rate and stable cycling performance.

GRAPHICAL ABSTRACT

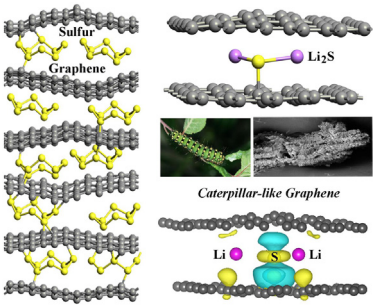

ARTICLE INFO

Article history:
Received 1 March 2017
Received in revised form 30 March 2017
Accepted 10 April 2017
Available online 12 April 2017

Keywords:
Lithium sulfur batteries
Shuttle effect
Reconfigurable graphene
Mass loading
Density functional theory

ABSTRACT

Lithium sulfur batteries, one of the most promising energy storage methodologies for emerging electric vehicles, suffer from poor long-term cycling stability due to the shuttle effect caused by the dissolution of high order polysulfides. To enhance the cycling stability of sulfur cathode for high-energy lithium sulfur batteries, it is very critical to mitigating the dissolution of polysulfides. In this work, a caterpillar-like and reconfigurable graphene was designed to serve as the sulfur host. The caterpillar-like graphene highly expanded in solution and tightly restacked in dry condition due to the van der Waals force. Elemental sulfur was trapped and confined inside the restacked graphene layers. High mass loading of 63.8% sulfur in graphene was achieved after the caterpillar-like graphene was dried at 155 °C. The graphene-sulfur electrode has a good rate performance of 708 mAh g^{-1} at 167.5 mA g^{-1}, 582 mAh g^{-1} at 335 mA g^{-1}, 470 mAh g^{-1} at 837.5 mA g^{-1}, 400 mAh g^{-1} at 1675 mA g^{-1} and a stable cycling performance with small capacity decay of 0.16% per cycle over 200 cycles at 1675 mA g^{-1}. Moreover, the underlying mechanism of the restacking effect of caterpillar-like graphene on immobilizing the soluble lithium polysulfides was studied by density functional theory (DFT), which clearly explained how the graphene immobilized the soluble lithium polysulfides by the restacking effect.

1. Introduction

Lithium ion batteries (LIBs) have been widely applied in mobile phone, computer and electric vehicle [1–4]. However, the traditional cathode materials based on the intercalation chemistry have a limited energy density [5]. Fortunately, the sulfur cathode can

* Corresponding authors.
E-mail addresses: h.zhu@neu.edu (H. Zhu), dh_msc@nuaa.edu.cn (H. Dou).
[1] These authors contributed equally to this work.

http://dx.doi.org/10.1016/j.cej.2017.04.052
1385-8947/

further promote the development of LIBs due to its high theoretical specific capacity of 1675 mAh g^{-1} [6–10]. Moreover, sulfur has advantages of low cost and environment-friendly property. However, lithium sulfur (Li-S) batteries based on the sulfur cathode and lithium anode still face some issues [11–15]. One is the low electronic conductivity of sulfur active materials, which leads to the low actual specific capacity [16–20]. The other is the soluble intermediate lithium polysulfides into the organic electrolyte, resulting in a low Coulombic efficiency and poor cycling performance [21–24].

Graphene is a promising sulfur host due to its high electronic conductivity, unique two-dimensional structure, and excellent mechanical flexibility [25,26]. A hierarchical porous graphene was designed as an electronic conduit to confine the active materials and act as a mini-electrochemical chamber for the reversible reactions of sulfur and lithium sulfide, showing an excellent electrochemical performance even at ultra-low temperature [27]. A porous graphene hydrogel [28] and mesoporous graphene paper [29] as free-standing sulfur hosts were demonstrated to effectively trap the soluble lithium polysulfides. However, the graphenes mentioned above trap the sulfur active materials by a weak physical adsorption. Thus the reported electrochemical results do not exceed more than 100 cycles. Therefore, the functional groups on the graphene surface are pretty important to further immobilize the soluble sulfur active materials [30]. Hydroxylated graphene showed a superior cycling performance due to the chemical adsorption on the graphene surface *via* functional groups [31,32]. Fang et al. [37] proposed an all-graphene structure sulfur cathode: a highly porous graphene (HPG) for a high sulfur content host, highly conductive graphene (HCG) for a current collector due to its high conductivity and light weight, and partially oxygenated graphene (POG) for the polysulfide adsorption layer, obtaining high specific capacities and stable cycling performance for LSBs. Moreover, nitrogen-doped graphene can chemically adsorb lithium polysulfides, which is resulted from the unique binding formation between the nitrogen functional group and lithium polysulfides, thus effectively improving the electrochemical performance of LSBs [33–36].

The restacking of graphene is inevitable in the synthesis process. However, the restacking effect on immobilizing the soluble lithium polysulfides is ignored. Therefore, the restacking effect of graphene on LSBs needs a thorough analysis and research. Herein, a caterpillar-like graphene was designed to act as a sulfur host. The caterpillar-like graphene was kept high expansion in solution, at which status the elemental sulfur was deposited. The graphene restacked under dry condition due to the pi interaction between the adjacent layers of graphene, and the sulfur was trapped and confined between the conductive graphene layers. Here, the mass loading of sulfur is 63.8%. The restacked graphene cage can provide high conductive networks and effectively confine the polysulfide intermediates during the electrochemical reaction in LSBs. Therefore, the graphene-sulfur cathode shows a high electrochemical rate capability and good cycling stability. Furthermore, the restacking effect of graphene on immobilizing the soluble lithium polysulfides was further studied by density functional theory.

2. Experimental section

2.1. Preparation of the graphene-sulfur composite

0.5 g of graphite and 2.8 g of anhydrous ferric chloride powders were heated at 380 °C for 24 h under the nitrogen atmosphere. Thus, the ferric chloride-intercalated graphite was obtained. 30 mg of $FeCl_3$-graphite was soaked in 10 ml of H_2O_2 (30%) at room temperature for 12 h to exfoliate. The obtained graphene was repeatedly washed with hydrochloric acid (37%), deionized water, ethanol, and toluene. Then, the graphene was dipped in the 22.5 mg sulfur of 5 mL toluene solution. After evaporating the toluene, the graphene-sulfur composite was dried at 60 °C for 12 h and further treated at 155 °C for 10 h. The graphene-sulfur composite was obtained after it was cooled to room temperature.

2.2. Characterization

X-ray diffraction (XRD) patterns were measured on a Bruker-AXS D8 DISCOVER. Copper Kα line was used as a radiation source with λ = 0.15406 nm. Field emission scanning electron microscopy (FESEM) and transmission electron microscopy (TEM) measurements were carried out with JEOL JSM-6380LV FE-SEM and FEI TECNAI-20, respectively. Scanning transmission electronic microscope (STEM) was performed on a Tecnai G2 F30. The X-ray photoelectron spectroscopy (XPS) analysis was performed on a Perkin-Elmer PHI 550 spectrometer with Al Kα (1486.6 eV) as the X-ray source. The Raman spectra of graphene were measured by using a Jobin Yvon HR800 confocal Raman system with a 632.8 nm diode laser excitation on a 300 line S mm^{-1} grating at room temperature. Thermal gravimetric (TG) analysis was conducted on a TG-DSC instrument (NETZSCH STA 409 PC) under an N_2 atmosphere at a heating rate of 10 °C min^{-1} from 30 to 600 °C.

2.3. Electrochemical characterization

LIR2032-type coin cells were assembled and tested by the galvanostatic cycling to estimate the electrochemical performance of the graphene-sulfur composite. The working electrodes were prepared by a slurry coating procedure. The slurry consisted of 70 wt% active material, 20 wt% Super C65 and 10 wt% polyvinylidene fluoride (PVDF) dissolved in N-methyl pyrrolidinone (NMP), and was uniformly spread on an aluminum foil current collector. Finally, the electrode was dried at 60 °C overnight. Each current collector contained *ca* 2.0 mg cm^{-2} active material. Test cells were assembled in an argon-filled glove box using Li foil as the counter electrode and polypropylene (PP) film as the separator. The electrolyte was 1 mol L^{-1} LiTFSI and 0.2 mol L^{-1} $LiNO_3$ in a mixed solvent of 1, 3-dioxolane (DOL) and 1, 2-dimethoxyethane (DME) with a volume ratio of 1:1. The coin cells were galvanostatically charged-discharged at different current densities between 1.7 and 2.8 V (*vs.* Li/Li^+) using a CT2001A cell test instrument (LAND Electronic Co.). The cyclic voltammetry (CV) measurement was conducted with a Gamry Reference 3000 electrochemical workstation at a scan rate of 0.2 mV s^{-1} in the voltage range of 1.7–2.8 V (*vs.* Li/Li^+). Electrochemical impedance spectroscopy (EIS) was measured in the frequency range of 100 kHz–10 mHz with an amplitude of 5 mV.

2.4. Computational section

The theoretical calculations are carried out by using the Vienna Ab-initio Simulation Package (VASP), which is based on the density functional theory (DFT). DFT calculations are performed by using a plane wave based with a cutoff energy of 400 eV. Generalized gradient approximation (GGA) in the form of Perdew-Burke-Ernzerhof (PBE) [38] is employed as the exchange correlation potential. Van der Waals (vdW) corrections in the Grimme implementation (DFT-D2) [39] are also included. Brillouin zone is sampled by a 4*4*1 *k*-points mesh. A large lattice constant (17 Å) along the perpendicular direction of the atomic plane is utilized to eliminate the interaction between the graphene and the periodic image. The structures are fully optimized until none of the forces is exceeded 0.01 eV $Å^{-1}$.

3. Results and discussion

The graphite-$FeCl_3$ was obtained by heating the graphite and anhydrous ferric chloride in a two-zone reactive container (See experimental section). And the ferric chloride was intercalated between the graphite layers (Fig. 1a and d). Then, the hydrogen peroxide was added into the graphite-$FeCl_3$. In this process, a large amount of oxygen is produced, leading to the exfoliation of graphite to graphene due to the expansion. The reaction equation between $FeCl_3$ and H_2O_2 is proposed as following: [40]

$$FeCl_3 + H_2O_2 \rightarrow FeCl_2 + H_2O + O_2$$

The volume of the obtained graphene immensely expanded to more than 10 times bigger compared to that of the original graphite (Fig. 1b and e). Then, the aqueous solution in the graphene was replaced by a sulfur toluene solution. After a heat treatment at 150 °C, the volume of the obtained graphene-sulfur composite dramatically shrunk (Fig. 1f) due to the van der Waals between the neighboring graphene layers. Meanwhile, sulfur was confined between the graphene layers (Fig. 1c).

The morphology of the graphene was measured by scanning electron microscopy (SEM). The graphene is like a caterpillar (Fig. 2a), which shows laminar (red circles in Fig. 2b) and porous (white circles in Fig. 2b) structure under higher magnification. High-resolution SEM image further shows that the caterpillar-like graphene has a wrinkled structure (Fig. S1). After evaporating toluene, sulfur is uniformly dispersed in the interlayer of few layer graphene. There are no clear sulfur particles deviating from the graphene (Fig. 2c). Meanwhile, the porous graphene becomes more compact due to the pi interaction in the dry status (blue circle in Fig. 2d), effectively inhibiting the sulfur escaping from the graphene matrix. X-ray diffraction (XRD) pattern of the graphene exhibits a diffraction peak at 26° (Fig. 2e), corresponding to the (002) spacing of graphene stacks [41]. XRD pattern of sulfur exhibits two prominent peaks at 23° and 28° [42], which corresponds to an *Fddd* orthorhombic structure. Although the intensity of the XRD diffraction peaks of graphene-sulfur is weaker than those of sulfur, the peak positions of sulfur in graphene-sulfur sample have no change, indicating that sulfur exists in an *Fddd* orthorhombic state in the graphene-sulfur composite. We characterized the

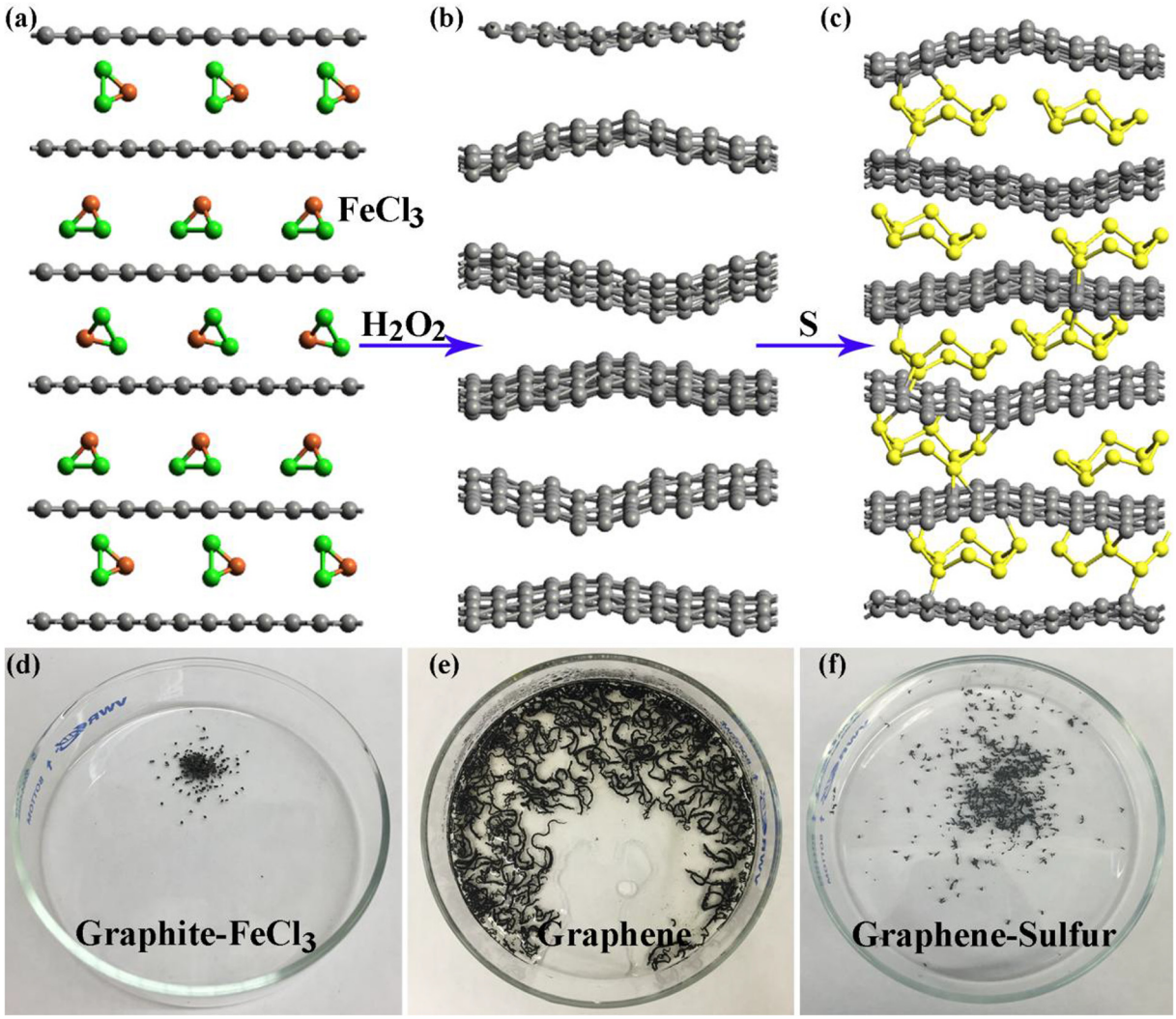

Fig. 1. Schematic illustrations of (a) graphite-$FeCl_3$, (b) graphene, and (c) graphene-sulfur. (a) The $FeCl_3$ is intercalated between the graphite layers: the red, green, and gray dots represent Fe, Cl, and C, respectively. (b) After $FeCl_3$ reacts with H_2O_2, the graphite is expanded to graphene. (c) Sulfur is confined between the graphenes after the heat treatment. The yellow dots represent S. Digital photographs of (d) graphite-$FeCl_3$, (e) graphene, and (f) graphene-sulfur. After $FeCl_3$ reacts with H_2O_2, the volume of graphene becomes larger compared that of the graphite. Then, the volume of graphene sharply shrinks after the sulfur encapsulation, indicating sulfur is confined between the graphenes. (For interpretation of the references to color in this figure legend, the reader is referred to the web version of this article.)

sulfur mass loading by thermal gravimetric (TG) analysis. One obvious weight loss from ~200 to 400 °C in the TG curve corresponds to the evaporation of sulfur, and the mass loading achieves 63.8% (Fig. 2f). Here, the capillary-like graphene reconfiguration plays a huge role and thus sulfur is largely confined in the graphene.

The caterpillar-like graphene consists of graphene nanosheets, which is a promising substrate for the reversible deposition/reactions of sulfur active materials (Fig. 3a). The layer distance is 0.393 nm in three layer graphene which is larger than 0.34 nm of graphite (Fig. 3b), indicating the graphite was successfully exfoliated by the above chemical method. Sulfur is homogeneously confined on the surface of the graphene (Fig. 3c). The nanosheet structure of graphene still remains after the sulfur encapsulation. The layer distance of graphene-sulfur is 0.42 nm (Fig. S3), indicating that graphene expands after sulfur intercalation. Energy dispersive X-ray (EDX) elemental mapping images further confirm that sulfur uniformly distributes in the graphene (Fig. 3d), indicating that sulfur has an intimate contact with the graphene nanosheet. Thus, the caterpillar-like graphene can act as a high conductive "*work platform*" for the reversible reactions of sulfur active materials.

Cyclic voltammetry (CV) curves of the graphene-sulfur electrode for LSBs clearly show two pairs of oxidation-reduction peaks (Fig. 4a) [43]. One pair of oxidation-reduction peaks at 2.4 and 2.3 V corresponds to the reversible reactions between S_8 and Li_2S_n ($4 \leq n \leq 8$). The other pair of oxidation-reduction peaks at 2.3 and 2.0 V is ascribed to the reversible reactions between Li_2S_n and

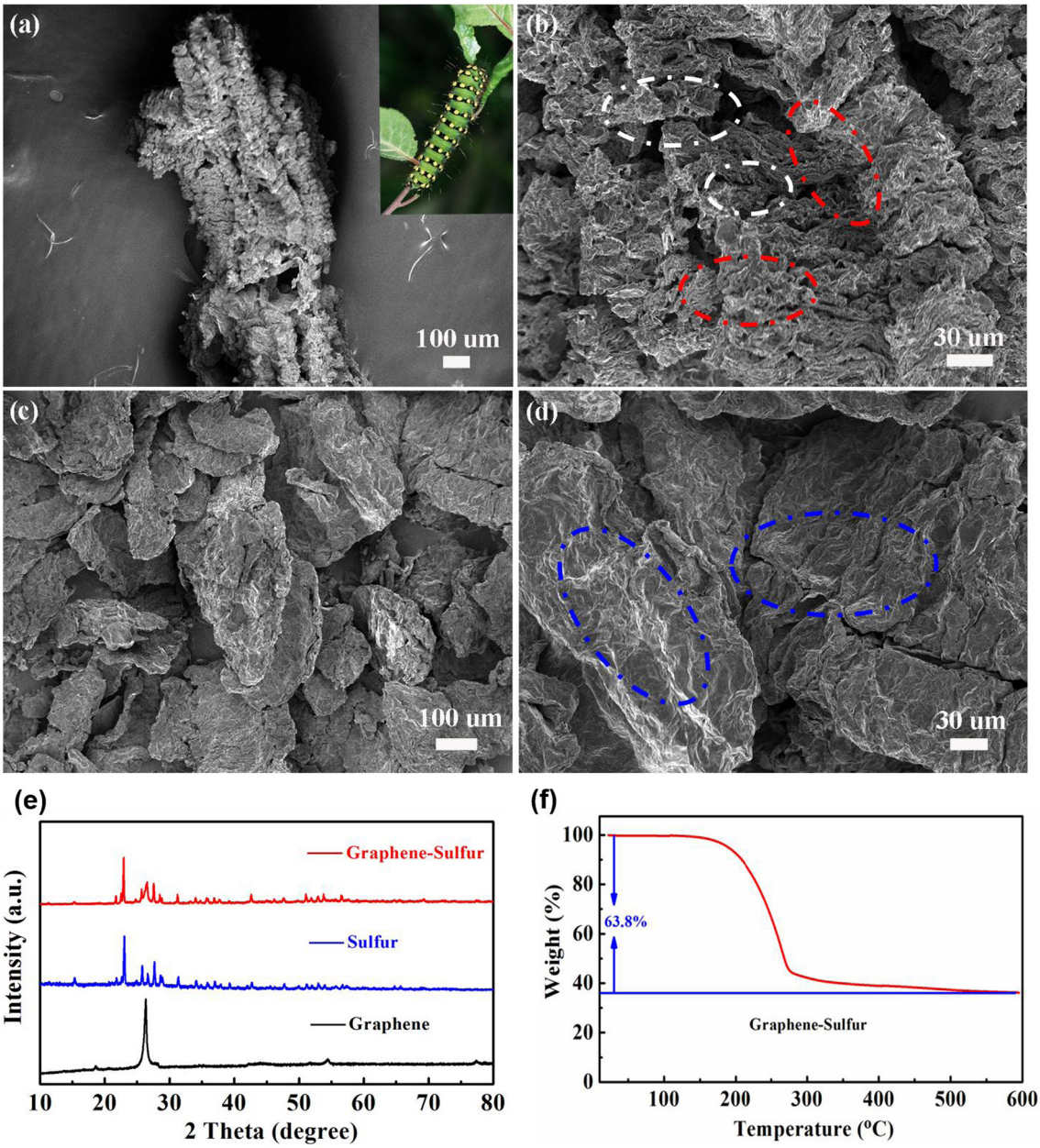

Fig. 2. SEM images of (a, b) graphene and (c, d) graphene-sulfur. (a, b) The graphene is like a caterpillar, which is composed of the laminated graphene. The inset in a is the digital photograph of a caterpillar. The red and white circles in b show the hierarchical and porous structure in the graphene individually. (c) There are no large sulfur particles on the graphene, indicating sulfur is uniformly dispersed in the graphene. (d) The blue circle in d presents that the graphene becomes more compact after the 155 °C heat treatment. (e) XRD patterns of graphene, sulfur, and graphene-sulfur composite. (f) TG curve of the graphene-sulfur. The sulfur content in the graphene-sulfur composite is 63.8%. (For interpretation of the references to color in this figure legend, the reader is referred to the web version of this article.)

Li_2S_2/Li_2S. The voltage potentials, peak currents, and peak areas of the CV curves are almost overlapped after the first cycle, indicating that the graphene-sulfur electrode has a stable cycling performance. The galvanostatic discharge curves of the graphene-sulfur electrode at different rates exhibit two plateaus (Fig. 4b). The first discharge plateau at ~2.3 V can be assigned to the open ring reduction of S_8 to lithium polysulfides (Li_2S_n, $4 \leq n \leq 8$). The second discharge plateau at ~2.1 V corresponds to Li_2S_n to Li_2S_2/Li_2S. These two plateaus correspond to the reduction reactions of sulfur and agree well with the two reduction peaks in the CV curves. Even at a high current density of 1 C (1 C = 1675 mA g^{-1}), the two plateaus still exist, indicating the graphene-sulfur electrode has a good rate performance. The graphene-sulfur electrode has an initial discharge capacity of 708 mAh g^{-1} at 0.1 C, 582 mAh g^{-1} at 0.2 C, 470 mAh g^{-1} at 0.5 C, and 400 mAh g^{-1} at 1 C (Fig. 4c). When the current density recovers to 0.1 C, the specific capacity is up to 522 mAh g^{-1}, showing a good rate performance of the graphene-sulfur electrode as a cathode for LSBs. The Coulombic Efficiency at low current density is lower than that at high current density. This can be attributed to the relatively rapid charge/discharge process at a high current rate [44], and polysulfide ions are not immediately dissolved into the electrolyte with the restacking effect of graphene. The shuttle effect is suppressed so that the Coulombic Efficiency is improved. This phenomenon also results that the cycling performance of graphene-sulfur electrode at high current density is more stable than that at low current density. Moreover, the graphene-sulfur electrode has an initial discharge capacity of 531 mAh g^{-1} (1094 mAh cm^{-3}) and retains 363 mAh g^{-1} (748 mAh cm^{-3}) after 200 cycles at a high current density of 1675 mA g^{-1}, exhibiting a stable cycling performance with a small capacity decay rate of 0.16% per cycle and a high Coulombic efficiency of 98.4% (Fig. 4d).

Density functional theory (DFT) calculations were performed to investigate the influence of the restacking effect on immobilizing the soluble lithium polysulfides [45]. A 5*5*1 supercell with a vacuum region of 15 Å was selected to investigate the adsorption mechanism of lithium polysulfides. Monolayer graphene is firstly investigated as a reference of the conventional graphene sulfur host (Fig. 5). The Li_2S molecule is adsorbed on the graphene surface by fixing two Li atoms at neighboring hollow sites (Fig. 5a). The height of Li atom on the graphene is 2.40 Å. The stability of the composite structure is analyzed by evaluating the binding energy, which is defined as the energy difference between the composite system and the individual components (graphene and lithium polysulfides). The binding energy is evaluated to be 0.70 eV. The value is slightly larger than the result (0.60 eV) of the previous report [33] due to the inclusion of van der Waals corrections. Electron difference densities for Li_2S on graphene are displayed in Fig. 5b. Few electrons accumulate between the lithium and carbon atom, indicating a weak adsorption interaction between Li_2S and the monolayer graphene.

Differently, the lithium polysulfides are sandwiched between two graphene layers in the caterpillar-like graphene system. The optimized schematic structures of Li_2S and LiS^* (This structure represents the other polysulfides: Li_2S_n, n = 2, 4, 6, 8.) embedded between two graphene layers are plotted in Fig. 6a and b, respectively. The Li_2S and LiS^* bind well with one graphene layer by the S-C bond and the bond distances are 1.90 and 1.95 Å, respectively. The bending of other graphene layer forms a small cap to bundle the lithium polysulfides in a small space. Electron difference

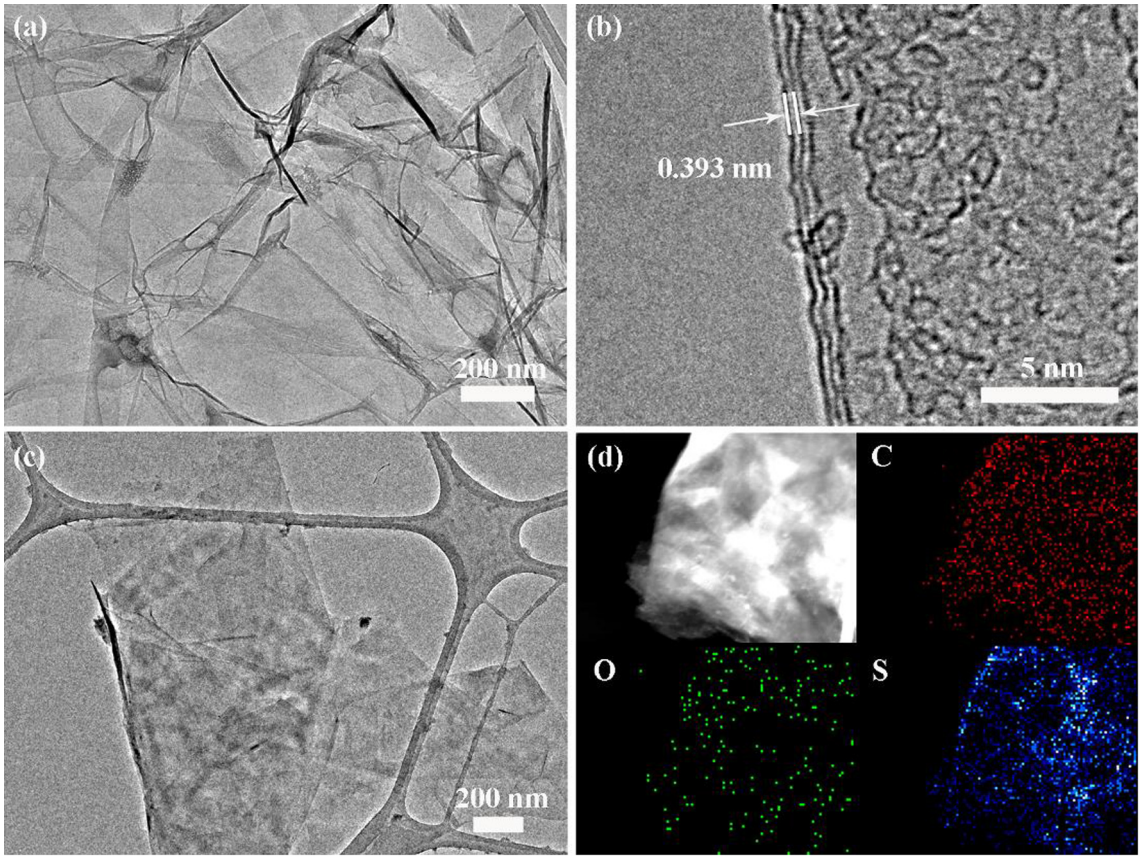

Fig. 3. TEM images of (a, b) graphene and (c) graphene-sulfur, and (d) corresponding elemental mapping images of carbon, oxygen and sulfur. (a, b) The graphene shows a plicated and layered structure. (c) There is no sulfur accumulation on the graphene. (d) STEM images further indicate the uniform dispersion of sulfur (Red represents carbon. Green represents oxygen. Blue represents sulfur). (For interpretation of the references to color in this figure legend, the reader is referred to the web version of this article.)

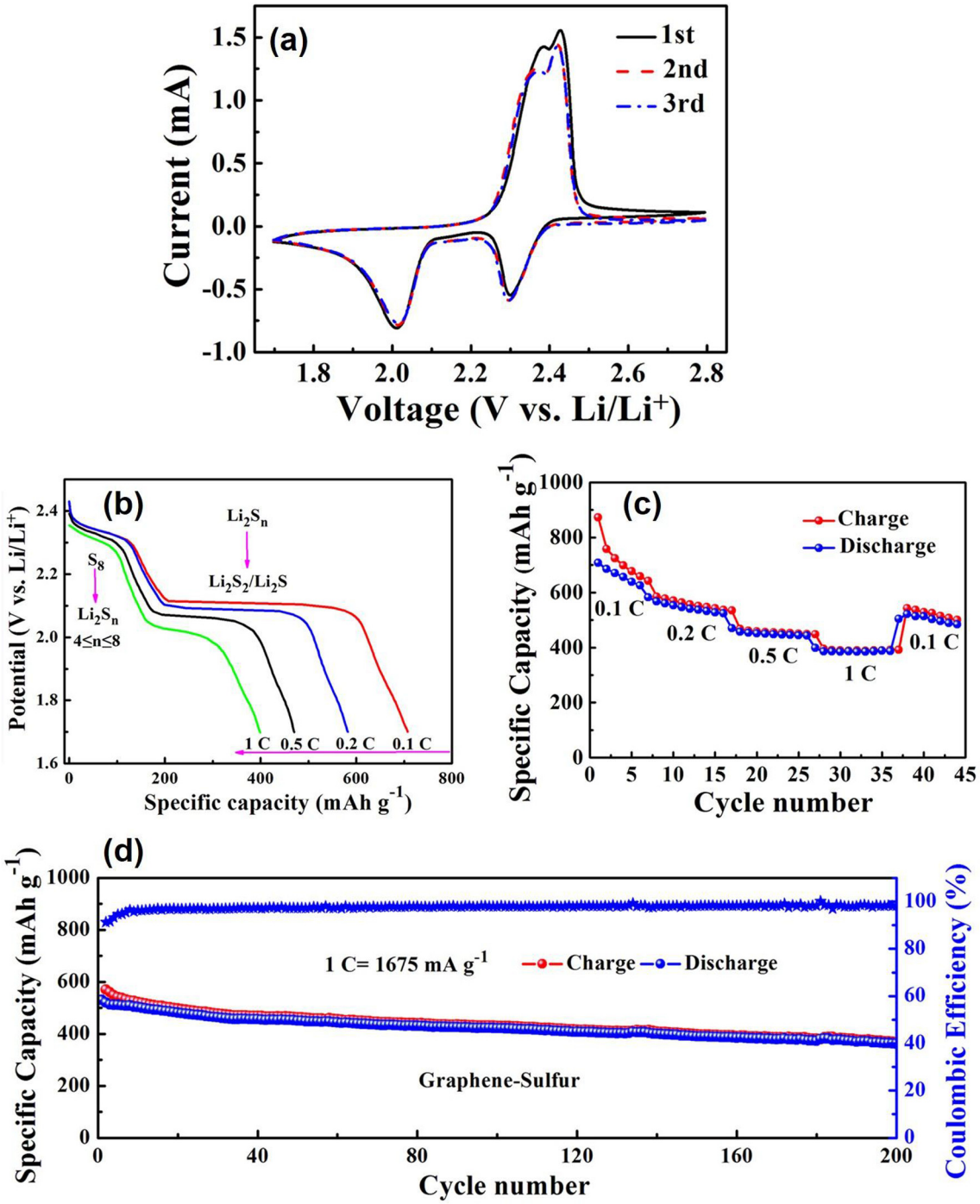

Fig. 4. (a) Typical CV curves of the graphene-sulfur electrode at a scan rate of 0.2 mV s^{-1}. (b) Galvanostatic discharge profiles of the graphene-sulfur electrode at different rates. The first discharge plateau at ~2.3 V can be assigned to the open ring reduction of S_8 to lithium polysulfides (Li_2S_n, $4 \leq n \leq 8$). The second discharge plateau at ~2.1 V corresponds to Li_2S_n to Li_2S_2/Li_2S. Even at a high current density of 1675 mA g^{-1}, the two plateaus still exist, indicating the graphene-sulfur electrode has a good rate performance. (c) Rate capability, and (d) cycling performance of the graphene-sulfur electrode at 1 C.

densities for the two systems defined as the difference between the charge density of the combined system and the densities of the individual components (i.e., polysulfides molecule and bilayer graphene) are shown in Fig. 6c, d. The graphene layers gain some electron from the Li atom and some electron accumulates around sulfur atom due to the high electronegativity of sulfur and carbon atom. Furthermore, the electrons accumulate between the sulfur and carbon atom, implying that a strong covalent bond is formed between sulfur and carbon atoms. The strong S-C bonding interaction from bottom layer combined with small cap effect form the upper layer causes a stronger anchoring between polysulfides molecule and bilayer graphene. Hence, the adsorption mechanism is different from that in the system of lithium polysulfides on a monolayer graphene (mentioned above). The binding energies are evaluated to be 2.01 and 1.77 eV for Li_2S and LiS^*, which are larger than that of monolayer system (0.70 eV). The binding energy between lithium polysulfides and graphene is higher, and the binding capability of graphene to lithium polysulfides is stronger, thus decreasing the dissolution of lithium polysulfides into the liquid electrolyte and increasing the cycling performance of LSBs

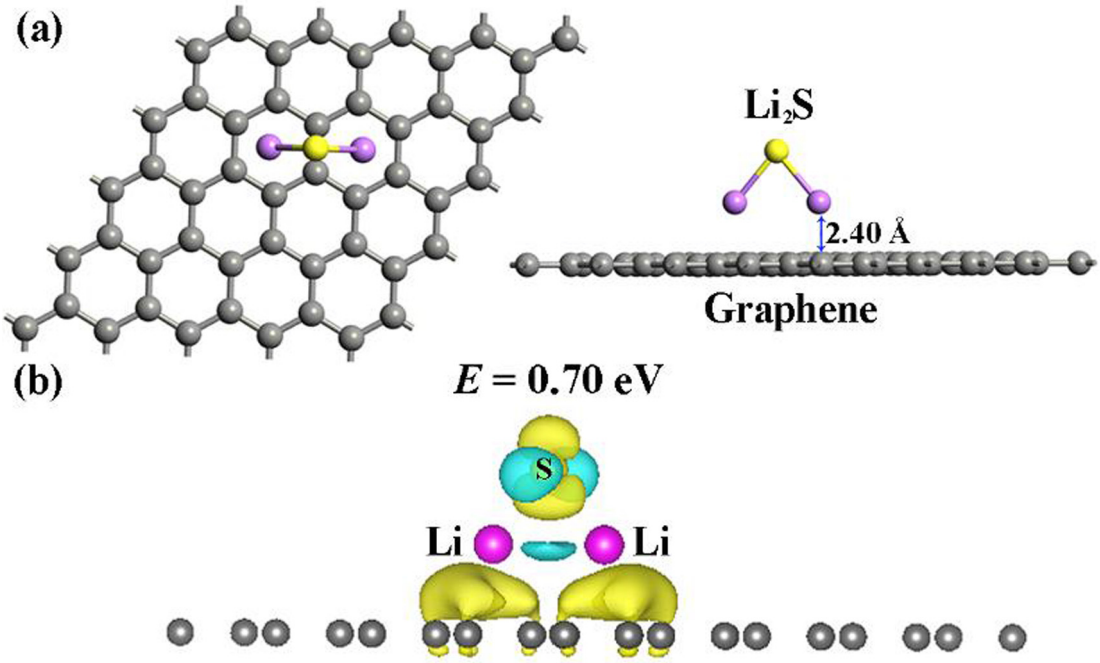

Fig. 5. (a) The schematic structure of Li_2S on a monolayer graphene. (b) Electron difference densities for Li_2S. The yellow and blue isosurfaces denote the electron accumulation and electron depletion zones, respectively. (For interpretation of the references to color in this figure legend, the reader is referred to the web version of this article.)

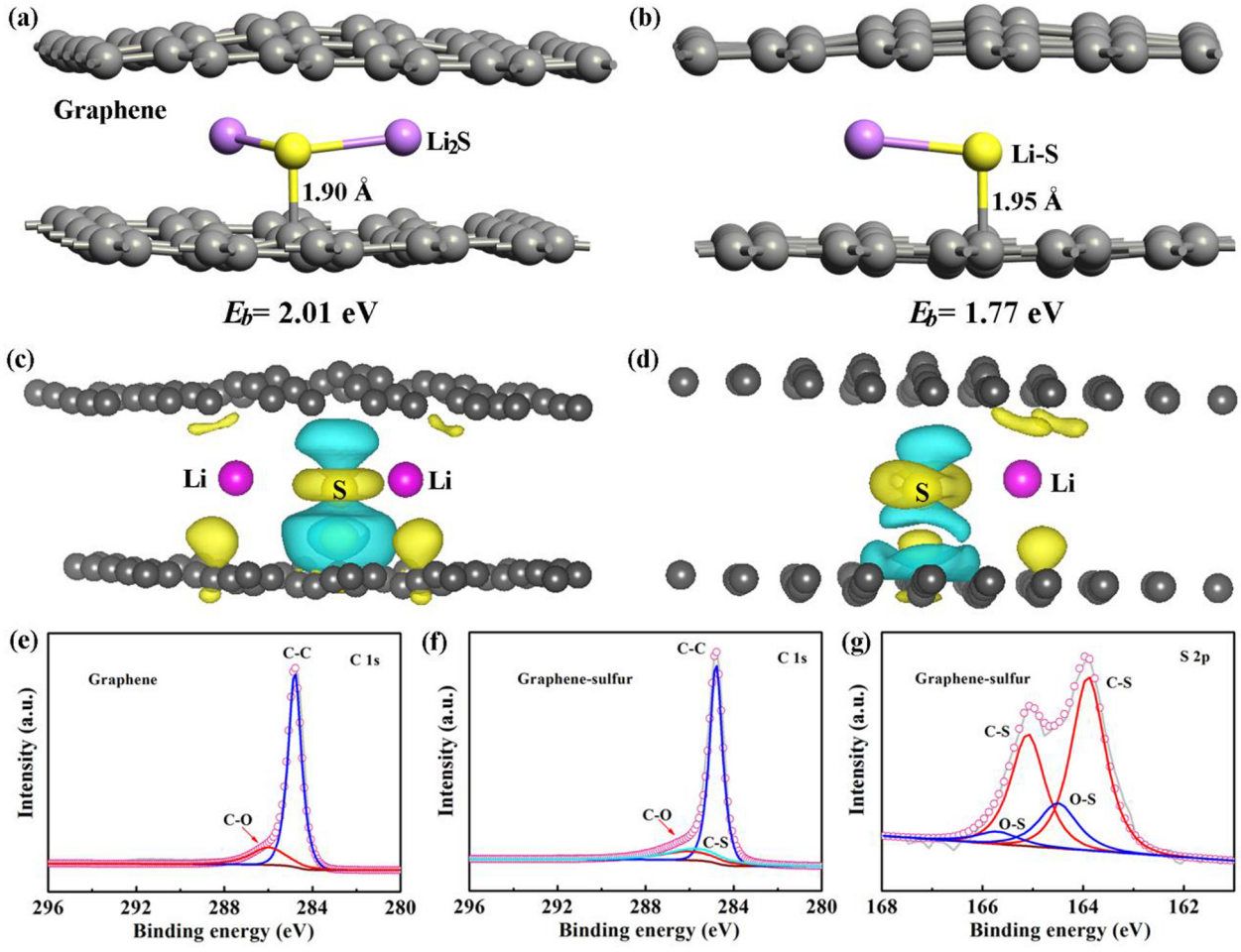

Fig. 6. The schematic structures of (a) Li_2S and (c) LiS^* sandwiched between two graphene layers. Electron difference densities for (c) Li_2S and (d) LiS^*. The yellow and blue isosurfaces denote the electron accumulation and electron depletion zones, respectively. The isosurface value of 0.0075 e $Å^{-3}$ is chosen. (e) C 1s XPS spectra for graphene. (f) C 1s and (g) S 2p XPS spectra for graphene-sulfur.

[33,43]. XPS was carried out to analyze the carbon bond in graphene. In the C 1 s spectra of graphene, the peaks at 284.8 and 286.0 eV correspond to the C–C bond and the C–O bond, respectively (Fig. 6e) [46,47]. However, an additional peak at 285.7 eV in the C 1s spectra of graphene-sulfur is attributed to the C–S bond (Fig. 6f) [48]. As shown in the S 2p spectra of graphene-sulfur (Fig. 6g), the peaks at 163.9 and 165.1 eV are assigned to the C-S bond [49]. The peaks at 164.5 and 165.7 eV correspond to the O–S bond. The XPS observation agrees well with the density functional theory calculations.

4. Conclusions

In summary, we prepared a caterpillar-like graphene as a sulfur host, with 63.8% sulfur mass loading. With the highly conductive graphene reconfiguration, the sulfur was confined in the graphene cage and achieved a high rate performance of 708 mAh g^{-1} at 167.5 mA g^{-1}, 582 mAh g^{-1} at 335 mA g^{-1}, 470 mAh g^{-1} at 837.5 mA g^{-1}, 400 mAh g^{-1} at 1675 mA g^{-1}. Owning to sulfur confining in the graphene cage, the sulfur had a good cycling stability of 363 mAh g^{-1} (748 mAh cm^{-3}) at 1675 mA g^{-1} for 200 cycles. Meanwhile, we demonstrated the restacking effect on immobilizing the soluble lithium polysulfides by a theoretical calculation. The result in this study is not only important for fundamental study in lithium sulfur batteries, but also inspiring of using highly conductive and reconfigurable graphene for sulfur encapsulating. Based on this work, a general way is provided to entrap of active materials (such as metallic oxide, metal sulfide and so on) by the van der Waals restacking effect in the caterpillar-like graphene for wide applications in electrochemical energy storage system, photocatalysis, and drug delivery.

Acknowledgements

H.L. Zhu acknowledges the startup support from Northeastern University. We acknowledge Dr. J. Li in MIT for sharing lab facilities. The authors are also grateful to the Natural Science Foundation of China (NSFC11374162) and Jiangsu Province (No. BK20151468). G.Y. Xu would like to thank Funding of Outstanding Doctoral Dissertation in NUAA (BCXJ15-07).

Appendix A. Supplementary data

Supplementary data associated with this article can be found, in the online version, at http://dx.doi.org/10.1016/j.cej.2017.04.052.

References

[1] T. Zhu, J.S. Chen, X.W. Lou, Glucose-assisted one-pot synthesis of FeOOH nanorods and their transformation to Fe_3O_4@carbon nanorods for application in lithium ion batteries, J. Phys. Chem. C 115 (2011) 9814–9820.
[2] C. Gong, Y.J. Bai, Y.X. Qi, N. Lun, J. Feng, Preparation of carbon-coated $MgFe_2O_4$ with excellent cycling and rate performance, Electrochim. Acta 90 (2013) 119–127.
[3] M. Yu, R. Li, M. Wu, G. Shi, Graphene materials for lithium-sulfur batteries, Energy Storage Mater. 1 (2015) 51–73.
[4] J. Liang, Z.H. Sun, F. Li, H.M. Cheng, Carbon materials for Li-S batteries: functional evolution and performance improvement, Energy Storage Mater. 2 (2016) 76–106.
[5] Z. Lin, Z. Liu, N.J. Dudney, C. Liang, Lithium superionic sulfide cathode for all-solid lithium-sulfur batteries, ACS Nano 7 (2013) 2829–2833.
[6] H. Wang, Y. Yang, Y. Liang, J.T. Robinson, Y. Li, A. Jackson, Y. Cui, H. Dai, Graphene-wrapped sulfur particles as a rechargeable lithium-sulfur battery cathode material with high capacity and cycling stability, Nano Lett. 11 (2011) 2644–2647.
[7] L. Suo, Y.S. Hu, H. Li, M. Armand, L. Chen, A new class of Solvent-in-Salt electrolyte for high-energy rechargeable metallic lithium batteries, Nat. Commun. 4 (2013) 1481.
[8] S. Zheng, F. Yi, Z. Li, Y. Zhu, Y. Xu, C. Luo, J. Yang, C. Wang, Copper-stabilized sulfur-microporous carbon cathodes for Li-S batteries, Adv. Funct. Mater. 24 (2014) 4156–4163.
[9] S. Zheng, Y. Wen, Y. Zhu, Z. Han, J. Wang, J. Yang, C. Wang, *In situ* sulfur reduction and intercalation of graphite oxides for Li-S battery cathodes, Adv. Energy Mater. 4 (2014), http://dx.doi.org/10.1002/aenm.201400482.
[10] J.S. Kim, T.H. Hwang, B.G. Kim, J. Min, J.W. Choi, A lithium-sulfur battery with a high areal energy density, Adv. Funct. Mater. 24 (2014) 5359–5367.
[11] V. Etacheri, R. Marom, R. Elazari, G. Salitra, D. Aurbach, Challenges in the development of advanced Li-ion batteries: a review, Energy Environ. Sci. 4 (2011) 3243–3262.
[12] C. Tang, Q. Zhang, M.Q. Zhao, J.Q. Huang, X.B. Cheng, G.L. Tian, H.J. Peng, F. Wei, Nitrogen-doped aligned carbon nanotube/graphene sandwiches: facile catalytic growth on bifunctional natural catalysts and their applications as scaffolds for high-rate lithium-sulfur batteries, Adv. Mater. 26 (2014) 6100–6105.
[13] C. Wang, X. Wang, Y. Yang, A. Kushima, J. Chen, Y. Huang, J. Li, Slurryless Li_2S/reduced graphene oxide cathode paper for high-performance lithium sulfur battery, Nano Lett. 15 (2015) 1796–1802.
[14] H. Kim, J.T. Lee, A. Magasinski, K. Zhao, Y. Liu, G. Yushin, *In situ* TEM observation of electrochemical lithiation of sulfur confined within inner cylindrical pores of carbon nanotubes, Adv. Energy Mater. 5 (2015), http://dx.doi.org/10.1002/aenm.201501306.
[15] D.R. MacFarlane, M. Forsyth, P.C. Howlett, M. Kar, S. Passerini, J.M. Pringle, H. Ohno, M. Watanabe, F. Yan, W. Zheng, S. Zhang, J. Zhang, Ionic liquids and their solid-state analogues as materials for energy generation and storage, Nat. Rev. Mater. 1 (2016) 15005.
[16] Z. Deng, Z. Zhang, Y. Lai, J. Liu, J. Li, Y. Liu, Electrochemical impedance spectroscopy study of a lithium/sulfur battery: modeling and analysis of capacity fading, J. Electrochem. Soc. 160 (2013) A553–A558.
[17] Z. Li, L. Yuan, Z. Yi, Y. Sun, Y. Liu, Y. Jiang, Y. Shen, Y. Xin, Z. Zhang, Y. Huang, Insight into the electrode mechanism in lithium-sulfur batteries with ordered microporous carbon confined sulfur as the cathode, Adv. Energy Mater. 4 (2014), http://dx.doi.org/10.1002/aenm.201301473.
[18] H. Yao, G. Zheng, P.C. Hsu, D. Kong, J.J. Cha, W. Li, Z.W. Seh, M.T. McDowell, K. Yan, Z. Liang, Improving lithium-sulphur batteries through spatial control of sulphur species deposition on a hybrid electrode surface, Nat. Commun. 5 (2014) 3943.
[19] D.S. Jung, T.H. Hwang, J.H. Lee, H.Y. Koo, R.A. Shakoor, R. Kahraman, Y.N. Jo, M. S. Park, J.W. Choi, Hierarchical porous carbon by ultrasonic spray pyrolysis yields stable cycling in lithium-sulfur battery, Nano Lett. 14 (2014) 4418–4425.
[20] W. Li, Z. Liang, Z. Lu, H. Yao, Z.W. Seh, K. Yan, G. Zheng, Y. Cui, A sulfur cathode with pomegranate-like cluster structure, Adv. Energy Mater. (2015), http://dx.doi.org/10.1002/AENM.201500211.
[21] X. Ji, K.T. Lee, L.F. Nazar, A highly ordered nanostructured carbon-sulphur cathode for lithium-sulphur batteries, Nat. Mater. 8 (2009) 500–506.
[22] C. Liang, N.J. Dudney, J.Y. Howe, Hierarchically structured sulfur/carbon nanocomposite material for high-energy lithium battery, Chem. Mater. 21 (2009) 4724–4730.
[23] D.W. Wang, Q. Zeng, G. Zhou, L. Yin, F. Li, H.M. Cheng, I.R. Gentle, G.Q.M. Lu, Carbon-sulfur composites for Li-S batteries: status and prospects, J. Mater. Chem. A 1 (2013) 9382–9394.
[24] S.S. Zhang, Sulfurized carbon: a class of cathode materials for high performance lithium/sulfur batteries, Front. Energy Res. 1 (2013) 10.
[25] J. Zhu, D. Yang, Z. Yin, Q. Yan, H. Zhang, Graphene and graphene-based materials for energy storage applications, Small 10 (2014) 3480–3498.
[26] G. Xu, Q.B. Yan, A. Kushima, X. Zhang, J. Pan, J. Li, Conductive graphene oxide-polyacrylic acid (GOPAA) binder for lithium-sulfur battery, Nano Energy 31 (2017) 568–574.
[27] J.Q. Huang, X.F. Liu, Q. Zhang, C.M. Chen, M.Q. Zhao, S.M. Zhang, W. Zhu, W.Z. Qian, F. Wei, Entrapment of sulfur in hierarchical porous graphene for lithium-sulfur batteries with high rate performance from −40 to 60 °C, Nano Energy 2 (2013) 314–321.
[28] G. Zhou, L.C. Yin, D.W. Wang, L. Li, S. Pei, I.R. Gentle, F. Li, H.M. Cheng, Fibrous hybrid of graphene and sulfur nanocrystals for high-performance lithium-sulfur batteries, ACS Nano 7 (2013) 5367–5375.
[29] X. Huang, B. Sun, K. Li, S. Chen, G. Wang, Mesoporous graphene paper immobilised sulfur as a flexible electrode for lithium-sulfur batteries, J. Mater. Chem. A 1 (2013) 13484–13489.
[30] J.W. Kim, J.D. Ocon, D.W. Park, J. Lee, Functionalized graphene-based cathode for highly reversible lithium-sulfur batteries, ChemSusChem 7 (2014) 1265–1273.
[31] L. Ji, M. Rao, H. Zheng, L. Zhang, Y. Li, W. Duan, J. Guo, E.J. Cairns, Y. Zhang, Graphene oxide as a sulfur immobilizer in high performance lithium/sulfur cells, J. Am. Chem. Soc. 133 (2011) 18522–18525.
[32] C. Zu, A. Manthiram, Hydroxylated graphene-sulfur nanocomposites for high-rate lithium-sulfur batteries, Adv. Energy Mater. 3 (2013) 1008–1012.
[33] Y. Qiu, W. Li, W. Zhao, G. Li, Y. Hou, M. Liu, L. Zhou, F. Ye, H. Li, Z. Wei, S. Yang, W. Duan, Y. Ye, J. Guo, Y. Zhang, High-rate, ultralong cycle-life lithium/sulfur batteries enabled by nitrogen-doped graphene, Nano Lett. 14 (2014) 4821–4827.
[34] G. Zhou, E. Paek, G.S. Hwang, A. Manthiram, Long-life Li/polysulphide batteries with high sulphur loading enabled by lightweight three-dimensional nitrogen/sulphur-codoped graphene sponge, Nat. Commun. 6 (2015) 7760.
[35] J. Song, Z. Yu, M.L. Gordin, D. Wang, Advanced sulfur cathode enabled by highly crumpled nitrogen-doped graphene sheets for high-energy-density lithium-sulfur batteries, Nano Lett. 16 (2016) 864–870.
[36] Z. Wang, Y. Dong, H. Li, Z. Zhao, H. Bin Wu, C. Hao, S. Liu, J. Qiu, X.W. Lou, Enhancing lithium-sulphur battery performance by strongly binding the

discharge products on amino-functionalized reduced graphene oxide, Nat. Commun. 5 (2014) 5002.
[37] R. Fang, S. Zhao, S. Pei, X. Qian, P.X. Hou, H.M. Cheng, C. Liu, F. Li, Toward more reliable lithium-sulfur batteries: An all-graphene cathode structure, ACS Nano 10 (2016) 8676–8682.
[38] J.P. Perdew, K. Burke, M. Ernzerhof, Generalized gradient approximation made simple, Phys. Rev. Lett. 77 (1996) 3865–3868.
[39] S. Grimme, Semiempirical GGA-type density functional constructed with a long-range dispersion correction, J. Comput. Chem. 27 (2006) 1787–1799.
[40] X. Geng, Y. Guo, D. Li, W. Li, C. Zhu, X. Wei, M. Chen, S. Gao, S. Qiu, Y. Gong, L. Wu, M. Long, M. Sun, G. Pan, L. Liu, Interlayer catalytic exfoliation realizing scalable production of large-size pristine few-layer graphene, Sci. Rep. 3 (2013) 1134.
[41] G. Xu, B. Ding, P. Nie, L. Shen, H. Dou, X. Zhang, Hierarchically porous carbon encapsulating sulfur as a superior cathode material for high performance lithium-sulfur batteries, ACS Appl. Mater. Interfaces 6 (2013) 194–199.
[42] F. Wu, J. Chen, R. Chen, S. Wu, L. Li, S. Chen, T. Zhao, Sulfur/polythiophene with a core/shell structure: Synthesis and electrochemical properties of the cathode for rechargeable lithium batteries, J. Phys. Chem. C 115 (2011) 6057–6063.
[43] G. Xu, J. Yuan, X. Tao, B. Ding, H. Dou, X. Yan, Y. Xiao, X. Zhang, Absorption mechanism of carbon-nanotube paper-titanium dioxide as a multifunctional barrier material for lithium-sulfur batteries, Nano Res. 8 (2015) 3066–3074.
[44] G. Xu, B. Ding, L. Shen, P. Nie, J. Han, X. Zhang, Sulfur embedded in metal organic framework-derived hierarchically porous carbon nanoplates for high performance lithium-sulfur battery, J. Mater. Chem. A 1 (2013) 4490–4496.
[45] W. Kohn, A.D. Becke, R.G. Parr, Density functional theory of electronic structure, J. Phys. Chem. 100 (1996) 12974–12980.
[46] Y. Xu, K. Sheng, C. Li, G. Shi, Self-assembled graphene hydrogel via a one-step hydrothermal process, ACS Nano 4 (2010) 4324–4330.
[47] L. Zhang, L. Ji, P.A. Glans, Y. Zhang, J. Zhu, J. Guo, Electronic structure and chemical bonding of a graphene oxide-sulfur nanocomposite for use in superior performance lithium-sulfur cells, Phys. Chem. Chem. Phys. 14 (2012) 13670–13675.
[48] K.H. Lee, P.E. Schwenn, A.R.G. Smith, H. Cavaye, P.E. Shaw, M. James, K.B. Krueger, I.R. Gentle, P. Meredith, P.L. Burn, Morphology of all-solution-processed "bilayer" organic solar cells, Adv. Mater. 23 (2011) 766–770.
[49] M.S. Park, J.S. Yu, K.J. Kim, G. Jeong, J.H. Kim, Y.N. Jo, U. Hwang, S. Kang, T. Woo, Y.J. Kim, One-step synthesis of a sulfur-impregnated graphene cathode for lithium-sulfur batteries, Phys. Chem. Chem. Phys. 14 (2012) 6796–6804.